J. Fluid Mech. (1996), vol. 324, pp. 287 308

The motion of an ellipsoid in tube flow at low Reynolds numbers

By MASAKO SUGIHARA-SEKI

Kansai University, Faculty of Engineering, Suita, Osaka 564, Japan
e-mail: sekim@gep.kansai-u.ac.jp

(Received 15 November 1994 and in revised form 14 May 1996)

The motion of a rigid ellipsoidal particle freely suspended in a Poiseuille flow of an incompressible Newtonian fluid through a narrow tube is studied numerically in the zero-Reynolds-number limit. It is assumed that the effect of inertia forces on the motion of the particle and the fluid can be neglected and that no forces or torques act on the particle. The Stokes equation is solved by a finite element method for various positions and orientations of the particle to yield the instantaneous velocity of the particle as well as the flow field around it, and the particle trajectories are determined for different initial configurations. A prolate spheroid is found to either tumble or oscillate in rotation, depending on the particle–tube size ratio, the axis ratio of the particle, and the initial conditions. A large oblate spheroid may approach asymptotically a steady, stable configuration, at which it is located close to the tube centreline, with its major axis slightly tilted from the undisturbed flow direction. The motion of non-axisymmetric ellipsoids is also illustrated and discussed with emphasis on the effect of the particle shape and size.

1. Introduction

In a recent paper, we presented a numerical study of the motion of an elliptical cylinder in a Poiseuille flow between two parallel plates in the limit of Stokes flow (Sugihara-Seki 1993). It was found that a cylinder that is freely suspended in a Poiseuille flow either tumbles or oscillates in rotation. In the tumbling motion, the particle rotates continuously with angular velocity in the direction of the vorticity; in the oscillatory motion, the particle periodically swings about a particular lateral position, changing its direction of rotation during a certain part of each period.

In this paper we extend the numerical study to a three-dimensional case. We consider the motion of a neutrally buoyant ellipsoidal particle in a narrow tube, with negligible inertial effects. This type of flow is encountered in a broad range of biological and engineering fields; examples include blood flow in the microcirculation, flow due to the motion of proteins in various biomedical applications, and the dynamics of solute molecules through pores or capsules flowing through tubes or pipes.

Early studies of the motion of a particle under the effect of walls were reviewed by Happel & Brenner (1983), and Clift, Grace & Weber (1978). The method of reflections furnishes a basis for the analysis of wall effects, as long as the particle dimensions are small with respect to the tube diameter. More recent developments including numerical methods in Stokes flow are discussed by Kim & Karrila (1991).

One of the simplest configurations considered by previous authors concerns the axisymmetric motion of a particle, or a periodic array of particles, along the axis of a circular tube. Wang & Skalak (1969) treated an infinite line of spheres located at the tube centreline using a singularity method, and Leichtberg, Pfeffer & Weinbaum (1976) considered the flow past a finite coaxial array of spheres. With regard to the motion of ellipsoids in tube flow, Wakiya (1957) expressed the flow around a single spheroid in a cylindrical tube using ellipsoidal harmonics, based on the classical solution by Oberbeck (1876), when the axis of revolution is along the tube centreline. A periodic array of spheroids located at the tube centreline was studied using a singularity method and a lubrication approximation by Chen & Skalak (1970). These studies of axisymmetric configurations do not involve rotary motions of the particle, as expected from symmetry.

A few studies have considered the motion of a particle located at an off-axis position in a tube. The flow of eccentric, closely fitting spheres in a tube is treated by Bungay & Brenner (1973) using a singular perturbation technique, and the flow of a spherical particle placed slightly off the axis is considered by Tözeren (1982), as a regular perturbation of the axisymmetric problem. In these configurations, a spherical particle freely suspended in tube flow exhibits no lateral motion.

Analyses using lubrication theory for closely fitting particles within a tube have also mainly treated steady motion, free of any lateral migration and rotation (Tözeren & Skalak 1978; Secomb *et al.* 1986). Exceptions are the studies of Hsu & Secomb (1989) and Secomb & Hsu (1993), which considered the motion of non-axisymmetric particles resembling red cell shapes in capillaries, and the stability of the motion of axisymmetric particles at the tube axis, respectively.

Recent developments of computational techniques have enabled the efficient treatment of particle–boundary interactions in Stokes flow (see for example, Weinbaum, Ganatos & Yan 1990; Kim & Karrila 1991; Pozrikidis 1992; Zhou & Pozrikidis 1995). Pozrikidis (1994) studied the motion of spheroids in a channel with parallel-sided walls using a boundary integral equation method, and found that the behaviour of spheroids in shear flow is largely dependent on the particle aspect ratio and the particle size relative to the channel width. Hsu & Ganatos (1994) used the boundary integral technique to consider the motion of a neutrally buoyant spheroid freely suspended in shear flow adjacent to a plane wall, and found that the spheroid undergoes a periodical motion toward and away from the wall as it continually tumbles forward.

With regard to the motion of an ellipsoid in an unbounded simple shear flow, Jeffery (1922) solved exactly the Stokes equations in an analytical form for two cases: (*a*) an ellipsoid of revolution, i.e. a spheroid, and (*b*) a general (non-axisymmetric) ellipsoid, for the special case where the ellipsoid rotates about a principal axis that is permanently aligned with the undisturbed vorticity vector. In the first case, the motion of the spheroid was found to consist of a spin about the axis of symmetry, and a precession of this axis about the vorticity vector of the undisturbed flow. The solution for a general ellipsoid in the second case was shown to be identical to that governing the time evolution of the projection of the symmetry axis of the spheroid onto the plane of shear flow. According to Jeffery's analysis, an ellipsoid will continue such a periodic motion indefinitely, unless its motion is disturbed by fluid and particle inertia, hydrodynamic or electrical interactions with nearby particles, Brownian rotations, or non-Newtonian properties of the suspending fluid.

The more general motion of non-axisymmetric ellipsoids in shear flow was studied by Hinch & Leal (1979), and their computation showed that the motion of an ellipsoid is doubly periodic: a relatively rapid rotation which corresponds to the motion of

axisymmetric particles around Jeffery orbits, and a slower drift which would be describable as a periodic change in the orbit if the particle were axisymmetric. Their examination of the stability of planar rotation about one of the principal axes of ellipsoids showed that the particle can execute stable planar rotations if the intermediate axis is aligned with the undisturbed vorticity.

Effects of quadratic velocity profiles on the motion of a prolate spheroid were studied by Chwang (1975), who considered the motion of a force-free particle in an unbounded paraboloidal flow using the singularity method. It was found that a prolate spheroid rotates as if it were immersed in a linear shear flow with a shear rate equal to that of the paraboloidal flow evaluated at the centre of the particle, and translates along a straight path parallel to the main flow direction without any side drift, which is not necessarily required by reversibility of Stokes flow.

Experimental studies of the motion of a single rigid particle in the Stokes flow regime have been, to the author's knowledge, largely confined to axisymmetric particles in a very large domain compared to the particle size or near a single plane wall. As Bretherton (1962) showed theoretically, it was observed that the motion of a single axisymmetric particle in an unbounded simple shear flow is identical to that of spheroids, provided that the effective axis ratio is set equal to the actual axis ratio for spheroidal particles, but must be determined experimentally for other particle shapes. A series of experimental studies by Mason, Goldsmith and coworkers has shown that the motions of rods and discs in Couette flow or tube flow at very low Reynolds numbers are in excellent agreement with Jeffery's model if the value of effective axis ratio is determined experimentally from the period of the rotary motion (see, for example, Goldsmith & Mason 1967). Stover & Cohen (1990) carefully examined the motion of a rodlike particle suspended in a shear flow near a wall, and found that the particle exhibits a tumbling motion even if an end of the particle passes very close to the wall during its rotation. The period of rotation increases with decreasing the gap width between the particle and the wall. When the particle comes extremely close to the wall, with the axis of symmetry almost lying in the plane of the shear flow, an irreversible non-hydrodynamic interaction between the particle and the wall takes place, and moves the particle away from the wall to a point where the distance between the centre of the particle and the wall is nearly equal to a half of the particle length (pole vaulting interaction). After this 'pole vaulting' interaction, the particle was observed to continue in a reversible periodic tumbling motion.

In this paper we consider only the motion where two of the three principal axes of the ellipsoid lie in a plane containing the tube axis so that the fluid motion is symmetric with respect to this plane. This is mainly to simplify the computation, which enables us to halve the computational domain, and thus reduce the size of the memory by one quarter. Nevertheless, we believe that this assumption may be a good starting point for the analysis of the general motion of an ellipsoid in tube flow. Under the corresponding assumption, the motion of an ellipsoid in unbounded simple shear flow is known to be stable if the intermediate axis is parallel to the undisturbed vorticity, as mentioned above.

The instantaneous velocities of the particle at arbitrary positions and orientations, and the flow of the suspending fluid are solved numerically by a finite element method. Using the computed particle linear and angular velocities, the trajectories of the particle are determined for various initial lateral positions and orientations. The present work is aimed at elucidating the behaviour of an ellipsoid in tube flow, depending on the particle size, axis ratios and initial conditions.

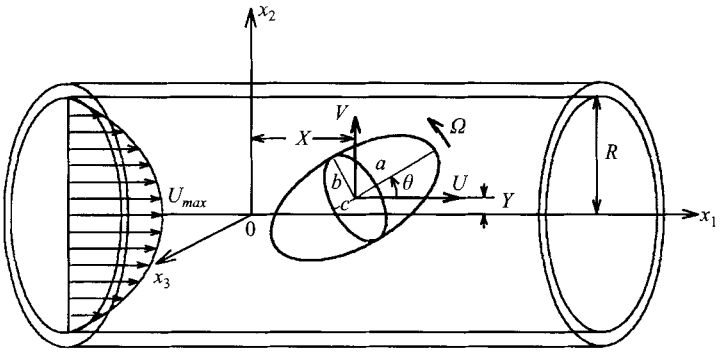

FIGURE 1. Configuration for an ellipsoid freely floating in a tube flow.

2. Formulation

Consider an ellipsoid with semi-axes a, b and c ($a \geqslant b$) in a tube with radius R (figure 1). The particle is assumed to be neutrally buoyant, and to move freely in a Poiseuille flow of an incompressible Newtonian fluid with viscosity μ. We assume that the principal axes a and b of the ellipsoid initially lie in a plane containing the tube axis, so that the configuration is symmetric with respect to the plane. In the present study, this condition is satisfied at any instant, because the translational velocity of the particle perpendicular to the plane and the components of the angular velocity in the plane always vanish, as expected from symmetry.

Expressing the maximum velocity of the undisturbed Poiseuille flow as U_{max}, we make all variables non-dimensional with respect to U_{max}, R and μ. Pressures and stresses are non-dimensionalized with respect to $\mu U_{max}/R$. A Cartesian coordinate system (x_1, x_2, x_3) fixed relative to the tube wall is introduced such that the x_1-axis is along the tube centre, and the (x_1, x_2)-plane coincides with the plane of symmetry containing the principal axes a and b of the ellipsoid. At any instant, the centre of the ellipsoid is at $(X, Y, 0)$, and the principal axis a forms an angle θ with the direction of the undisturbed stream.

We assume that the effects of inertial forces on the motion of the fluid and the particle are neglected. Thus, the fluid velocity $\boldsymbol{u}$ and the pressure p satisfy the Stokes equation and the continuity equation:

$$\nabla p = \nabla^2 \boldsymbol{u}, \tag{1}$$

$$\nabla \cdot \boldsymbol{u} = 0. \tag{2}$$

The velocity at the tube wall is zero, and the no-slip and no-penetration conditions are applied on the surface of the particle. The inflow and outflow boundaries are at a distance l upstream and downstream of the centre of the particle, where the Poiseuille velocity profile is assumed. In most cases, we adopted $l = 5$.

Since we have assumed that the inertial effects on the particle motion can be neglected, the resultant force $\boldsymbol{F}$ and torque $\boldsymbol{T}$ exerted on the particle by the fluid stresses on its surface vanish at every instant:

$$\boldsymbol{F} = \oint \boldsymbol{\sigma} \cdot \mathrm{d}\boldsymbol{s} = \boldsymbol{0}, \tag{3}$$

and

$$\boldsymbol{T} = \oint \boldsymbol{r} \times (\boldsymbol{\sigma} \cdot \mathrm{d}\boldsymbol{s}) = \boldsymbol{0}, \tag{4}$$

where $\boldsymbol{\sigma}$, $\boldsymbol{r}$ and $\mathrm{d}\boldsymbol{s}$ represent the stress tensor, the position vector relative to the centre of the particle, and a surface element of the particle, and the integrations are carried out over the surface of the particle. These quasi-steady conditions determine the translational velocity $\boldsymbol{U} = (U, V, 0)$ and the angular velocity $\boldsymbol{\Omega} = (0, 0, \Omega)$ of the particle. Note that the x_3-component of $\boldsymbol{U}$ and the x_1- and x_2-components of the angular velocity always vanish as noted before.

Since the flow is symmetric with respect to the (x_1, x_2)-plane, it is sufficient to consider half of the flow domain. Then the computational domain can be chosen as D $\{(x_1, x_2, x_3) : X - l \leqslant x_1 \leqslant X + l, (x_2^2 + x_3^2)^{1/2} \leqslant 1, x_3 \geqslant 0\}$. Given the position and orientation of the ellipsoid, its motion and the flow of the suspending fluid in the domain D are computed by a finite element method, based on a variational principle (Sugihara-Seki 1995). Briefly, a variational functional that produces the Stokes equation may be obtained as (Olson & Tuann 1978)

$$J = \int_D \left[\frac{1}{4}\left(\frac{\partial u_i}{\partial x_j} + \frac{\partial u_j}{\partial x_i}\right)^2 - p\frac{\partial u_i}{\partial x_i}\right] \mathrm{d}x_1 \mathrm{d}x_2 \mathrm{d}x_3. \tag{5}$$

Considering independent variations of $(\boldsymbol{u}, p)$ and $(\boldsymbol{U}, \boldsymbol{\Omega})$, the variation of J can be expressed as

$$\delta J = -\int_D \frac{\partial \sigma_{ij}}{\partial x_j} \delta u_i \, \mathrm{d}x_1 \mathrm{d}x_2 \mathrm{d}x_3 - \int_D \frac{\partial u_i}{\partial x_i} \delta p \, \mathrm{d}x_1 \mathrm{d}x_2 \mathrm{d}x_3 - F_i \delta U_i - T_i \delta \Omega_i. \tag{6}$$

Thus, requiring that J is stationary with respect to $(\boldsymbol{u}, p)$ and $(\boldsymbol{U}, \boldsymbol{\Omega})$ under appropriate boundary conditions yields equations (1), (2), (3), and (4) as the Euler equations of the variational principle.

In the numerical procedure, the domain D is divided into a number of finite elements. A typical grid is shown in figure 2. Each element has a hexahedral shape with 27 nodes including eight corner nodes (Sugihara-Seki 1995). Using the values of the velocity at the 27 nodes and the values of the pressure at the eight corner nodes, the velocity and pressure within each element are approximated by quadratic and linear functions in terms of local coordinates, respectively. The nodal values of $(\boldsymbol{u}, p)$ and $(\boldsymbol{U}, \boldsymbol{\Omega})$ are to be determined. Substituting the expressions for the velocity and pressure into equation (5), and following a variational principle, we obtain a set of linear equations for the nodal values of $(\boldsymbol{u}, p)$ and $(\boldsymbol{U}, \boldsymbol{\Omega})$. These equations are solved numerically using a Gaussian elimination method, under appropriate boundary conditions. A typical mesh has 432 elements, 4291 nodes and 9887 unknowns. A representative run with double-precision arithmetic takes approximately 300 s on a FACOM VP-2600 Computer at the Data Processing Centre, Kyoto University, Japan.

For several values of a, b and c, computations were carried out for various selected values of the lateral position Y and angle of inclination θ, in the physically accessible range of $0 \leqslant Y < 1$ and $0 \leqslant \theta \leqslant \pi/2$, to obtain the longitudinal, lateral and angular velocities of the particle, U, V and Ω. The equations of motion of the particle:

$$\frac{\mathrm{d}X}{\mathrm{d}t} = U, \qquad \frac{\mathrm{d}Y}{\mathrm{d}t} = V, \qquad \frac{\mathrm{d}\theta}{\mathrm{d}t} = \Omega, \tag{7}$$

are solved by Euler's method, and the trajectory of the particle is determined for various initial configurations.

In order to assess the numerical accuracy of the present finite element method, we

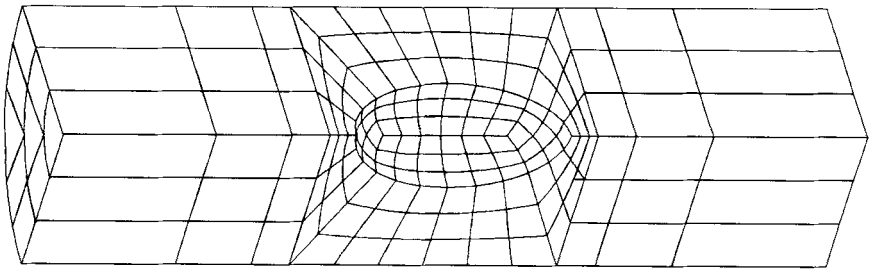

FIGURE 2. Typical grid for the finite element method. Only half of the computational domain ($x_2 \geqslant 0$) is shown for clarity.

compare our results with those of previous studies, for four cases: (i) a sphere placed at the tube centreline, (ii) a sphere placed slightly off-axis, (iii) a spheroid placed at the tube centreline with its symmetrical axis aligned to the undisturbed flow direction, and (iv) a small prolate spheroid in tube flow. Comparisons are made with the results of Wang & Skalak (1969), Chen & Skalak (1970) and Bungay & Brenner (1973) in case (i), Tözeren (1982) and Bungay & Brenner (1973) in case (ii), Wakiya (1957) and Chen & Skalak (1970) in case (iii), and Chwang (1975) in case (iv). In all cases, excellent agreement was obtained except for very small particles. The difference between the present solutions and the previous results for the translational and angular velocities of a spherical particle (cases (i) and (ii)) is within the order of 0.1% for $a < 0.9$, and it is less than 1.5% for $0.9 < a < 0.98$. The error of the translational velocity of a spheroid in case (iii) is less than 0.1%. In case (iv), the longitudinal and angular velocities of a prolate spheroid with $a = 0.3, b = c = 0.1$ at various orientations were found to agree with the analytical solutions for the particle in an unbounded paraboloidal flow within the order of 10^{-3}, and the lateral velocity was less than 10^{-5}, which should be exactly zero if it were immersed in an unbounded paraboloidal flow. These differences include the effect of the tube wall as well as numerical errors of the present scheme.

3. Particle velocities

The results of a typical run for a prolate spheroid with $a = 0.8$ and $b = c = 0.2$ are shown in figures 3(a) and 3(b), which show velocity vectors and pressure contours of the suspending fluid in the plane of symmetry $x_3 = 0$, and pressure contours on the particle surface. Since the particle is located at the tube centreline, it exhibits only a lateral motion with no rotation, as expected from symmetry and reversibility arguments. In this case, the particle moves upward. The flow patterns and pressure contours in the plane of symmetry shown in figure 3 are quite similar to those for the two-dimensional case (elliptic cylinders in channel flow) (see figure 5 in Sugihara-Seki 1993). The pressure distribution on the particle surface along the circumference at $x_3 = 0$, in particular, is very similar to that in the two-dimensional case.

Next, we consider the velocities of an ellipsoid and the pressure drop along the tube, at various configurations of the particle. Figure 4 shows the dimensionless velocities U, V, Ω, and the additional pressure drop $\Delta(p - p_0)$ due to the particle, for ellipsoids with $a = 0.8, b = 0.2$ and various values of c located at several lateral positions. Here, p_0 denotes the pressure in the absence of the particle (i.e. due to the undisturbed Poiseuille flow) and Δ denotes the difference between the upstream (at $x_1 = X - l$) and downstream values (at $x_1 = X + l$). The curves shown in

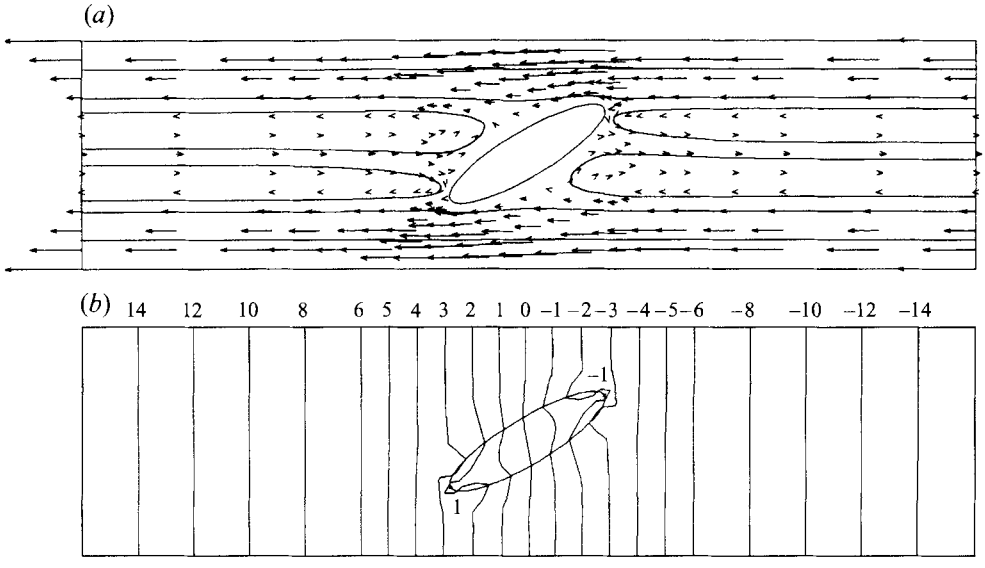

FIGURE 3. (*a*) Velocity vectors of the suspending fluid in the plane $x_3 = 0$ relative to the longitudinal velocity of a prolate spheroid with $a = 0.8$ and $b = c = 0.2$, located at the tube centreline with $\theta = \pi/6$. The solid curves represent some typical streamlines. (*b*) Pressure contours of the suspending fluid in the plane $x_3 = 0$, and those on the particle surface. The numbers denote the values of $p - p_m$, where p_m represents the average of the upstream (at $x_1 = X - l$) and downstream pressures (at $x_1 = X + l$).

figure 4 are quite similar in shape to the corresponding curves for elliptic cylinders in channel flow (see figures 6 and 7 in Sugihara-Seki 1993). As for large and/or slender elliptic cylinders, the angular velocity of the oblate spheroid becomes negative when it is located off the centre of the tube with its major axis almost aligned to the tube axis (see Figure 4*c*). Since the negative angular velocity of the particle can be explained in terms of a lubrication force generated between the particle and the tube wall (Sugihara-Seki 1993), it is reasonable that we are more likely to observe this phenomenon for ellipsoids with larger c. In figure 4, a notable difference between the two- and three-dimensional motion is that the lateral velocity V of the oblate ellipsoid at the tube centreline is negative at small inclinations (see figure 4*c*), while V of elliptic cylinders is positive for all orientations. A physical explanation of the negative lateral velocity of oblate spheroids at small orientations will be given in §4.2.

The dependence of the particle velocities U, V, Ω and the additional pressure drop $\Delta(p - p_0)$ on the particle size is comparable to that for elliptic cylinders reported in Sugihara-Seki (1993), and will not be repeated here. An interesting feature emerges by comparing the angular velocity of a prolate spheroid with that in an unbounded paraboloidal flow (see rectangles in figure 4*a*), corresponding to a particle with the same axis ratios that is very small relative to the tube radius. For small θ, the presence of the tube wall reduces the angular velocity of the particle, but it enhances the angular velocity when the major axis of the particle is oriented nearly perpendicular to the tube axis. This occurs because the longitudinal motion of the particle causes it to roll along the wall and this contribution to the angular velocity is in addition to the angular velocity induced by the shear flow in the absence of the wall. A similar phenomenon has been reported for spheroids near a plane wall (Hsu & Ganatos 1994).

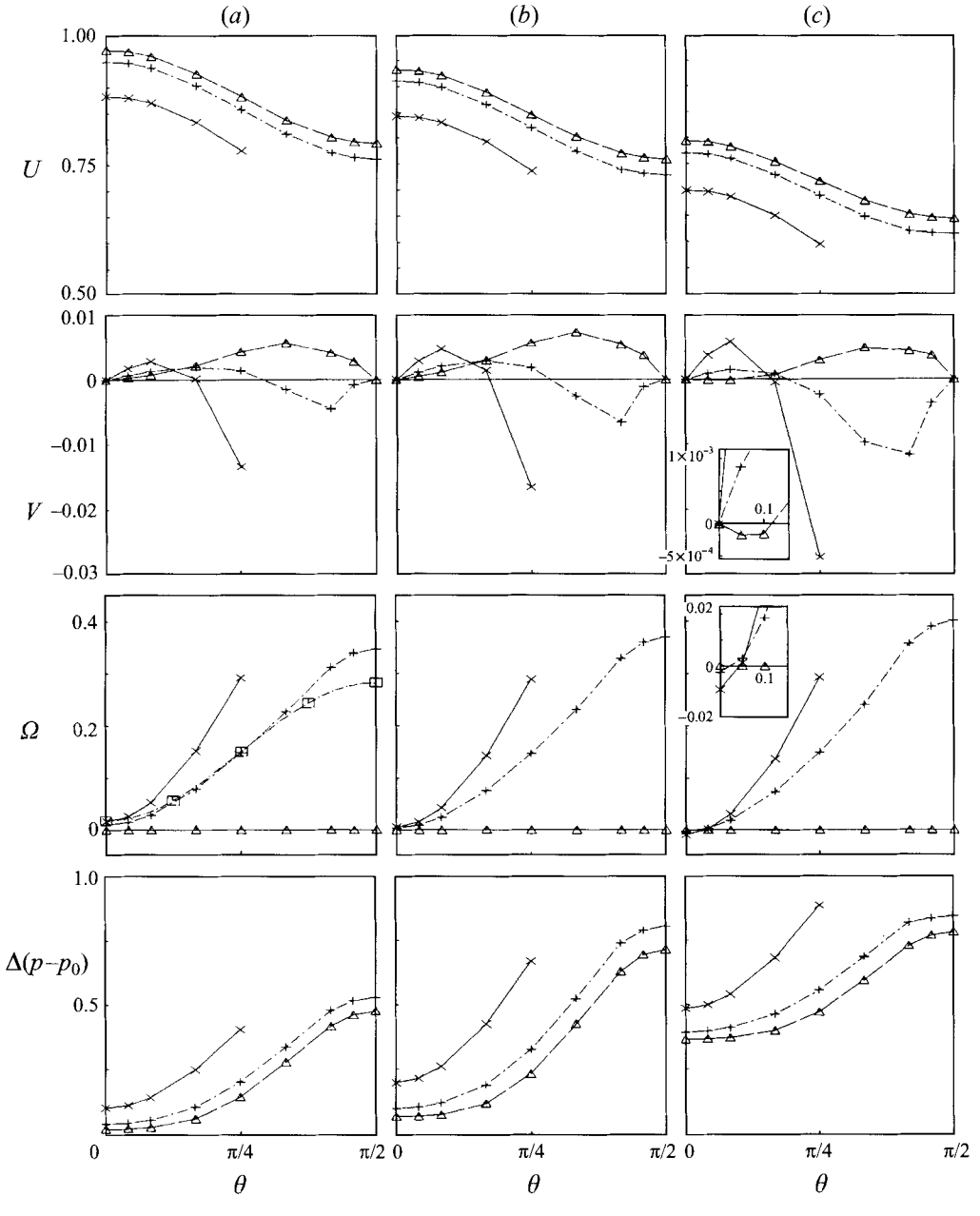

FIGURE 4. Particle velocities U, V, Ω and additional pressure drop $\Delta(p - p_0)$, for ellipsoids with $a = 0.8, b = 0.2$ and, (*a*) $c = 0.2$, (*b*) $c = 0.4$, and (*c*) $c = 0.8$, at lateral positions: $\triangle$, $Y = 0$; $+$, $Y = 0.15$; $\times$, $Y = 0.3$. In (*a*), rectangles represent the values of the angular velocity for a prolate spheroid with $a = 0.8, b = c = 0.2$ located at $Y = 0.15$ in an unbounded paraboloidal flow (Chwang 1975). In (*c*), the additional pressure drop is scaled down by a factor 0.4.

For the velocity component U, of great interest is the slip velocity U_s of the ellipsoid centre relative to the local fluid velocity of the undisturbed flow, i.e. $U_s = U - (1 - Y^2)$. Figure 5 shows the slip velocity as a function of the inclination angle θ for ellipsoids with $a = 0.8, b = 0.2$ and various values of c located at three lateral positions. The slip velocity is always negative for all orientations and lateral positions, indicating

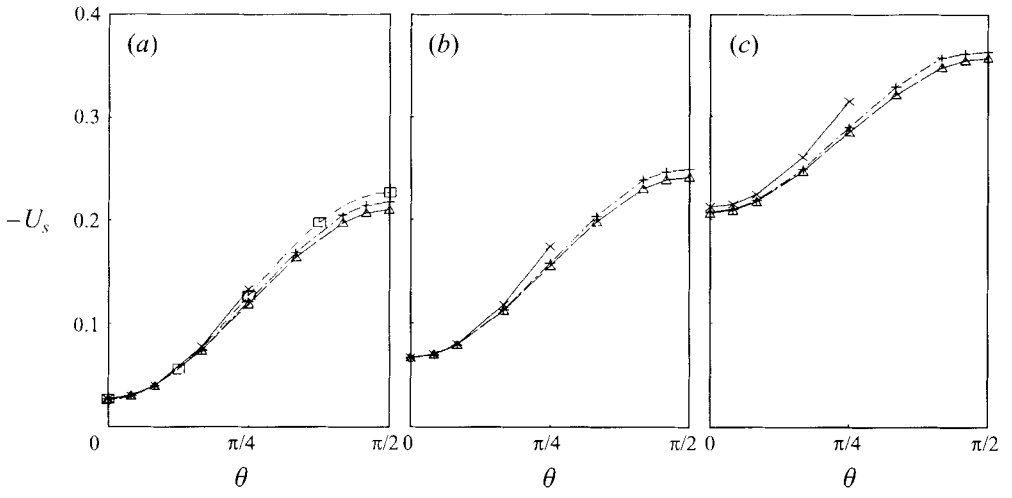

FIGURE 5. Slip velocity U_s for ellipsoids with $a = 0.8, b = 0.2$ and (*a*) $c = 0.2$, (*b*) $c = 0.4$, and (*c*) $c = 0.8$, at lateral positions: △, $Y = 0$; +, $Y = 0.15$; ×, $Y = 0.3$. In (*a*), rectangles represent the values of $-U_s$ for a prolate spheroid with $a = 0.8, b = c = 0.2$ in an unbounded paraboloidal flow (Chwang 1975).

that the ellipsoid always lags behind the fluid in tube flow. For a given lateral position, the ellipsoid experiences the minimum slip when its major axis is aligned with the direction of flow ($\theta = 0$), and its value is smaller for smaller c. Chwang (1975) obtained the velocity of a prolate spheroid freely floating in an unbounded paraboloidal flow, using the singularity method. His results of the slip velocity for a spheroid with $a = 0.8, b = c = 0.2$ are also shown in figure 5(*a*), for comparison. It is remarkable to observe that the slip velocities of a spheroid in an unbounded paraboloidal flow and in tube flow nearly coincide, unless the particle is located very close to the wall. In addition, the slip velocity of a particle in tube flow is almost insensitive to the lateral position, as it is for a prolate spheroid in unbounded paraboloidal flow (see equation (53) in Chwang 1975).

4. Particle trajectories

In a two-dimensional study, Sugihara-Seki (1993) has reported that an elliptic cylinder freely suspended in a Poiseuille flow between two parallel plates exhibits one of the following three types of motion, depending on the axis ratio and initial conditions: (i) continuous rotation about the direction of the vorticity; (ii) oscillation with its major axis swinging about $\theta = \pi/2$ and its centre swinging across the centreline; (iii) small-amplitude oscillation about $\theta = 0$. In type (iii) motion, the particle position is near the channel wall for small particles, while the oscillation is about the centreline for larger particles.

The present three-dimensional computations demonstrate that similar scenarios occur for prolate spheroids ($a > b = c$), whereas other types of motion can also occur for oblate spheroids ($a = c > b$). These two cases will be discussed separately, and the discussion of the motion of non-axisymmetric ellipsoids will follow.

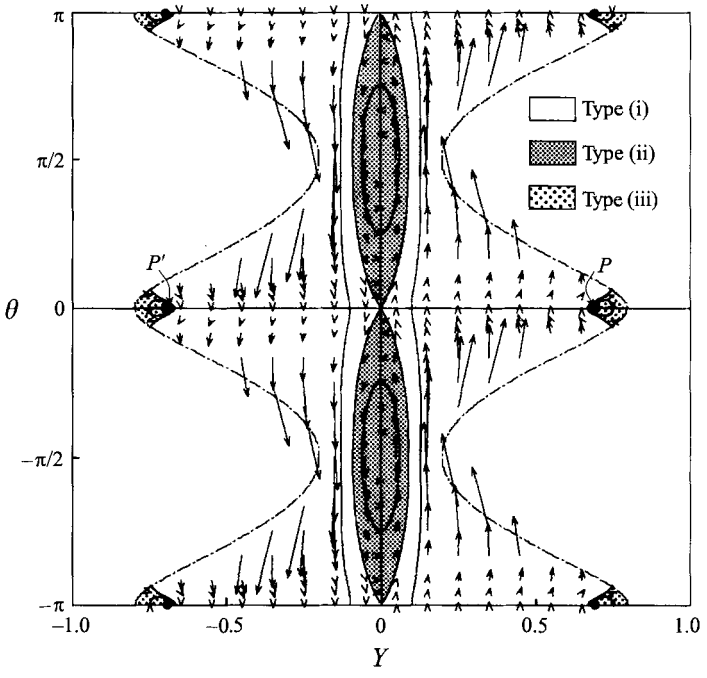

FIGURE 6. Lateral velocity V and angular velocity Ω of a prolate spheroid with $a = 0.8$ and $b = c = 0.2$. Each arrow shows a vector (V, Ω) when the lateral position and orientation of the particle are represented by the coordinates (Y, θ) at the origin of the arrow; —, temporal variations of the lateral position and orientation of the particle starting from various initial values; — · —, the critical configuration at which the particle touches the tube wall. The points P and P' represent configurations at which both of V and Ω vanish.

4.1. *Prolate spheroids*

In order to analyse the trajectories of a spheroid starting from various initial configurations, we plot vectors of (V, Ω) in the (Y, θ)-plane, for a prolate spheroid with $a = 0.8, b = c = 0.2$, in figure 6. Each arrow in figure 6 shows a vector (V, Ω) of the particle whose configuration is represented by the coordinates (Y, θ) at the origin of the arrow, and it represents the local direction of a particle trajectory in the (Y, θ)-plane. The solid curves show the temporal history of lateral position and orientation for some typical cases. A comparison with figure 9 in Sugihara-Seki (1993) shows that type (i), type (ii), and type (iii) motions are also present in the three-dimensional case. In the regions of motion type (iii), there are points P and P' where both V and Ω vanish, so that the particle motion is steady. Of course, the points $(Y, \theta) = (0, 0), (0, \pm\pi)$ and $(0, \pm\pi/2)$ represent steady configurations.

Typical examples of periodic evolutions of longitudinal and lateral positions and orientation $X/L, Y, \theta$, and the additional pressure drop $\Delta(p - p_0)$, as well as the particle velocities U, V, Ω are plotted over a period as a function of time t/T in figure 7. Here, T represents a period of motion, and L denotes the longitudinal distance at which the particle advances over a period. Figure 7 illustrates how the particle behaves in each type of motion. In the type (i) motion, the particle continuously rotates in the direction of the undisturbed vorticity. It can be shown that this rotary motion is approximated well by Jeffery's solution with a so-called effective axis ratio that is determined from the period of rotation. In the case of figure 7(*a*), the effective

axis ratio is evaluated to be approximately 6.44, which is larger than the actual axis ratio 4. It is found that the value of the effective axis ratio, or equivalently the period of tumbling motion, becomes larger as the particle approaches the tube wall. This tendency is consistent with the experimental observation of the motion of rods near a plane wall by Stover & Cohen (1990). Furthermore, as shown in figure 6, part of the ellipsoidal surface can come very close to the tube wall during a type (i) motion, and this may increase the possibility of some non-hydrodynamic interactions between the particle and the wall that are not considered in the present study. Such interactions may include the 'pole-vaulting' interaction of rods near a plane wall which is possibly caused by mechanical contact between the particle and wall (Stover & Cohen 1990).

Figure 7(*b*,*c*) shows that the type (ii) and (iii) motions are oscillatory, corresponding to closed loops of the particle trajectories in figure 6; in the type (ii) motion, the spheroid oscillates in rotation about $\theta = \pi/2$, swinging across the tube centreline; in the type (iii) motion, it oscillates about $\theta = 0$ with small amplitude, with its centre close to the tube wall. As a limiting case of the type (ii) motion, closed loops of the particle path in figure 6 are reduced to single points, $(Y, \theta) = (0, \pm\pi/2)$, where the particle remains at the centreline as expected from symmetry arguments. For the type (iii) motion, a limiting trajectory is represented by point P or P', where the particle is placed adjacent to the tube wall with its major axis aligned with the tube axis.

In all types of motion, the particle translates with a periodically varying longitudinal velocity, which is analogous to the jerking motion of a prolate spheroid in an unbounded paraboloidal flow (Chwang 1975). The ratios of the maximum and the minimum values of U over a period are approximately equal to 1.25, 1.13, and 1.46 for figure 7(*a*), 7(*b*) and 7(*c*), respectively. The considerable side drift observed in all three cases in figure 7 is apparently due to the presence of the tube wall: a spheroid in an unbounded paraboloidal flow has been reported to move along a straight path parallel to the undisturbed flow without any lateral motion (Chwang 1975).

In figure 8, the Y-coordinate of the point P, Y^*, is plotted as a function of a, for $a/b = 3$ and 4. The results for oblate spheroids and two-dimensional cases are also shown for comparison. In all cases, Y^* decreases with increasing a, until it reaches zero at a particular size, say the critical size $a^\dagger$, whose value depends on b and c. This result suggests that, as the particle size increases, the two separated regions of type (iii) motion near the Y-axis in the (Y, θ)-plane approach each other and touch the origin at $a = a^\dagger$. The behaviour of larger spheroids with a closer to $a^\dagger$ and larger than $a^\dagger$ will be discussed later with reference to figure 9. A comparison between two- and three-dimensional results in figure 8 demonstrates that Y^* is always larger in three than that in two-dimensional, for given values of a and a/b, suggesting that type (iii) motion is less favoured in the former case. Since the presence of type (iii) motion is closely related to the lubrication force generated in a narrow gap between the particle and the wall (Sugihara-Seki 1993), this tendency may result from the fact that in three-dimensional the fluid can go around the particle along its side and produce a weaker lubrication force.

Another interesting feature of figure 8 is that the value of Y^* for $a/b = 3$ is larger than that for $a/b = 4$ in the cases of two-dimensional and oblate spheroids, whereas the converse is true for prolate spheroids. This is presumably due to the effect of c: as shown later in figure 14(*a*), Y^* is, in general, smaller for larger c at given a and b. Since c is larger for prolate spheroids ($b = c$) with $a/b = 3$ than that for $a/b = 4$ at given a, the value of Y^* for $a/b = 3$ may be smaller than that for $a/b = 4$. It

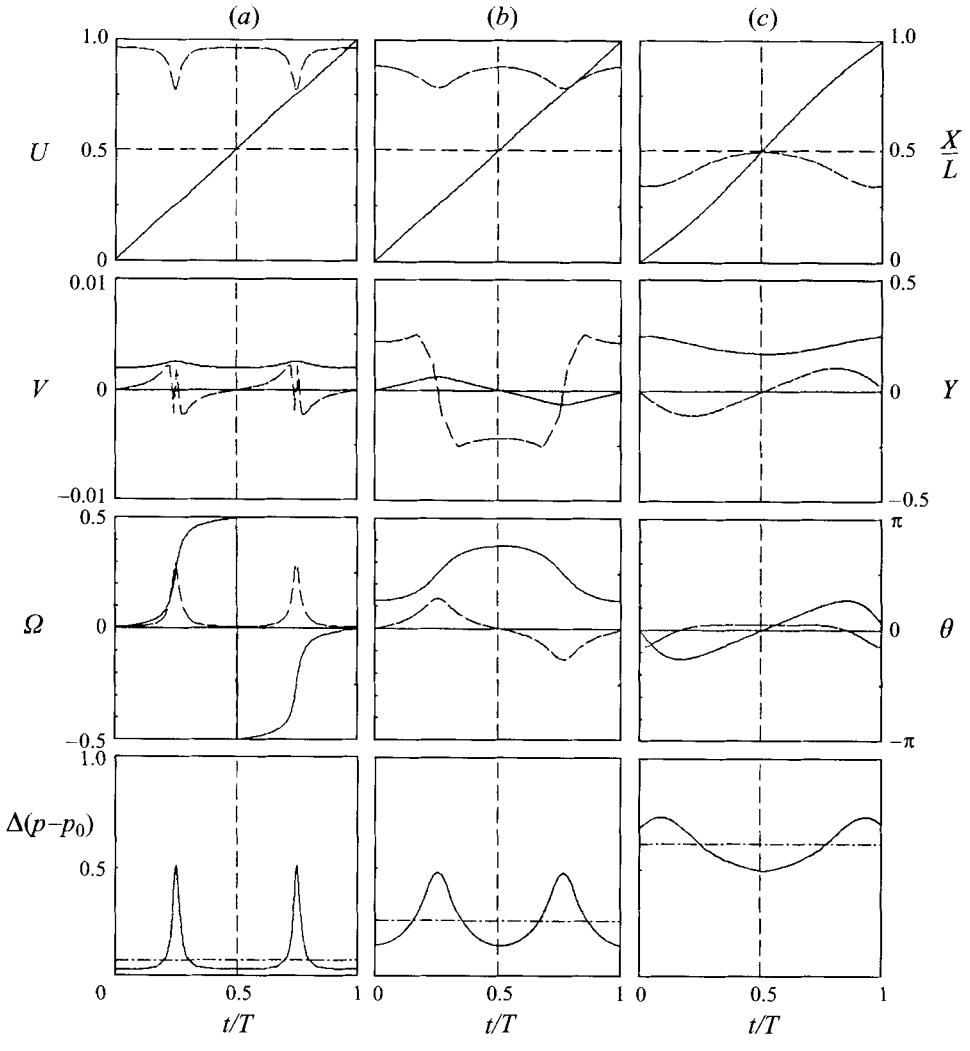

FIGURE 7. Time variations of the longitudinal and lateral positions $X/L, Y$, the orientation angle θ, and the additional pressure drop $\Delta(p - p_0)$, over a complete cycle for an ellipsoid with $a = 0.8, b = c = 0.2$. The time variations of the particle velocities U, V and Ω are also shown by dashed curves. (*a*) Type (i) motion starting from $(Y, \theta) = (0.1, 0)$, (*b*) type (ii) motion starting from $(0, \pi/4)$, and (*c*) type (iii) motion staring from $(0.75, 0)$. In (*c*), $Y - 0.5$ instead of Y is plotted, and Ω and θ are scaled up by a factor 10, for clarity. The dash-dotted curves represent the values averaged over the period of motion.

is apparent that this effect does not work for oblate spheroids ($c = a$) and elliptic cylinders in the two-dimensional case.

Type (i) and type (ii) motions are inhibited for ellipsoids with $a \geqslant 1$, because of the physical constraint that the particle cannot intersect the tube wall. In order to illustrate the motion of such large ellipsoids, figure 9(*a*) shows vectors of (V, Ω) and some representative trajectories for a spheroid with $a = 1$ and $b = c = 0.25$. Note that Y^* is positive (see figure 8) and the regions corresponding to type (i) and type (ii) motions still exist. Since type (i) and type (ii) motions are physically impossible in this case, we replace them by the new types (i′) and (ii′), respectively. In these regions,

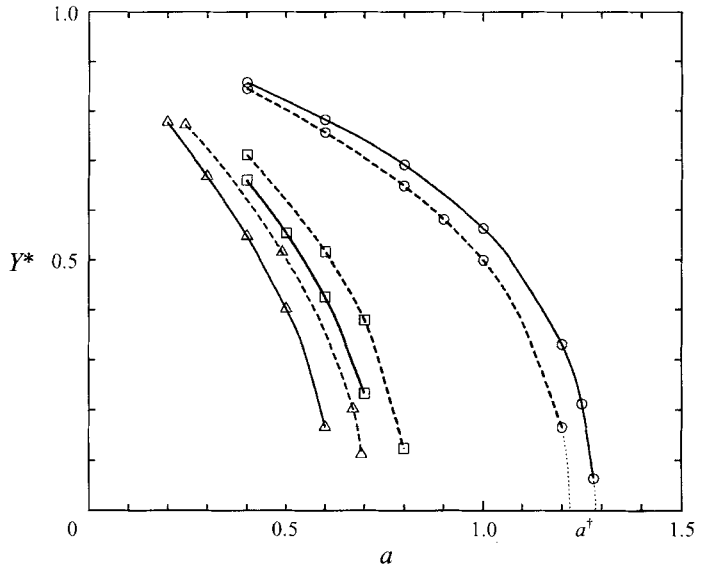

FIGURE 8. Lateral coordinates of point P, Y^*: ○, prolate spheroids ($a > b = c$); □, oblate spheroids ($a = c > b$); △, two-dimensional cases (elliptic cylinders in channel flow). Solid curves represent $a/b = 4$, and dashed curves $a/b = 3$.

the particle asymptotically approaches or departs from the point $(Y, \theta) = (0, \pi/2)$ or $(0, -\pi/2)$. These points represent the configuration at which both ends of the major axis of the spheroid touch the tube wall, with the axis perpendicular to the undisturbed flow.

Figure 9(*b*) shows the motion of a spheroid with $a = 1.6$ and $b = c = 0.4$. The particle is large enough that Y^* is no longer positive (see figure 8), so that the two separated regions of type (iii) motion near $\theta = 0$ in figures 6 and 9(*a*) are connected to one region covering the Y-axis in figure 9(*b*). In type (iii) motion, the oscillation is about the centreline, as is for large elliptic cylinders in the two-dimensional case. In type (ii′) motion, the particle asymptotically approaches or departs from the configuration at which both of upper and lower portions of the particle touch the tube wall, with its centre at the tube centreline. It is interesting to note that the origin in figures 6 and 9(*a*) is a saddle point, whereas the origin in figure 9(*b*) represents a neutrally stable configuration. This result for large prolate spheroids is in accord with that for closely fitting axisymmetric particles in tube flow studied by Secomb & Hsu (1993). It may be worth noting here that they suggest the possibility of oscillatory behaviour of a particle around this symmetrical configuration, which may correspond to the type (iii) motion shown in figure 9(*b*).

4.2. *Oblate spheroids*

Vectors of (V, Ω) and some representative trajectories for a spheroid with $a = c = 0.7$ and $b = 0.175$ are shown in figure 10. A striking feature is the presence of point Q on the θ-axis between 0 and $\pi/2$, say $\theta = \theta^*$, where both V and Ω vanish. As a result, a new type of motion, called type (iv) motion, can occur near the origin in the (Y, θ)-plane. Here, the particle traces a closed loop about the origin moving in

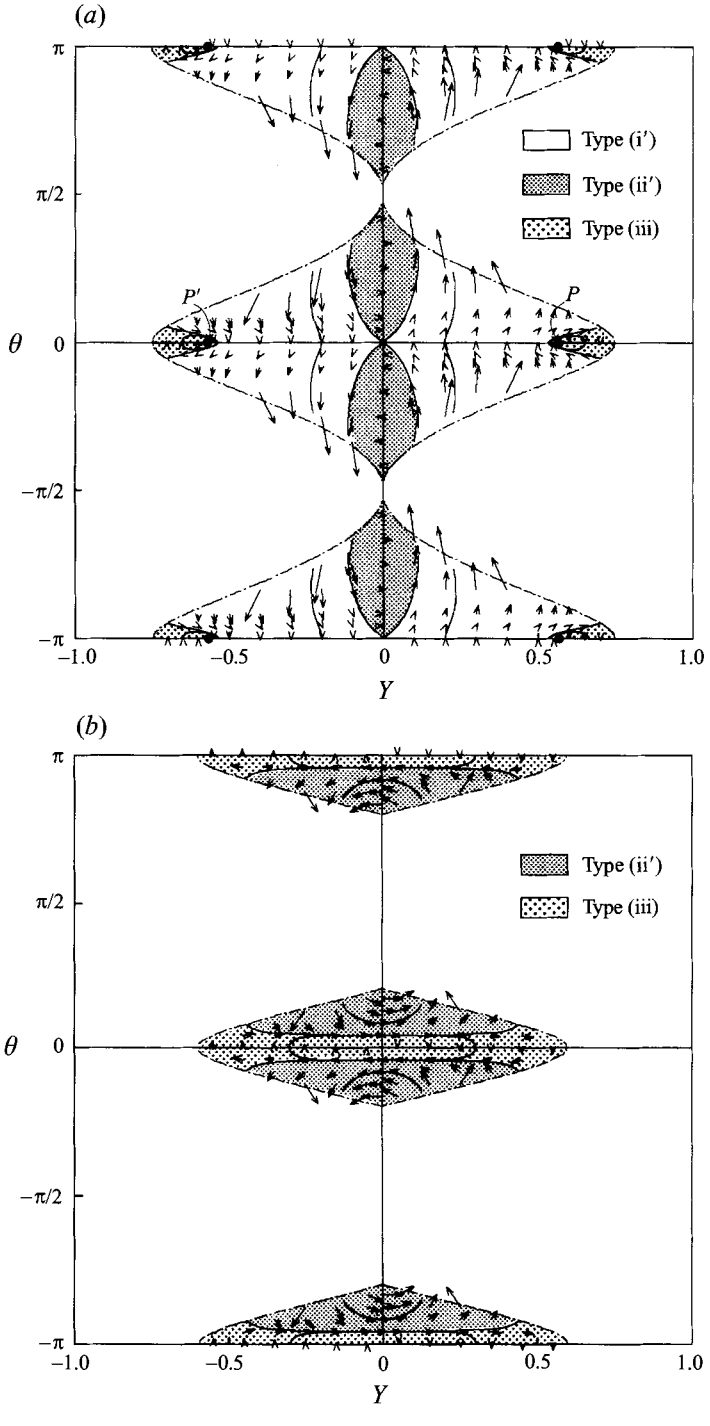

FIGURE 9. Vectors (V, Ω) for prolate spheroids: (*a*) $a = 1.0$, $b = c = 0.25$, (*b*) $a = 1.6$, $b = c = 0.4$.

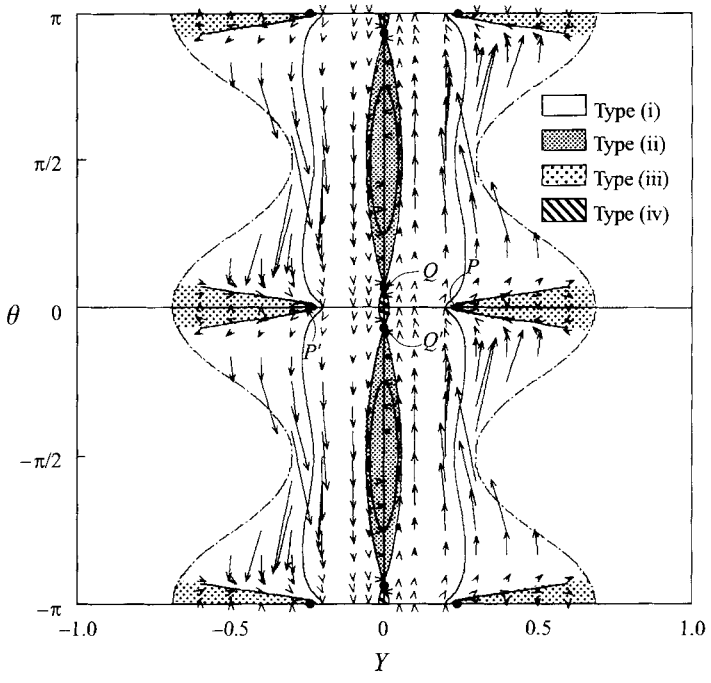

FIGURE 10. Vectors (V, Ω) for an oblate spheroid with $a = c = 0.7$ and $b = 0.175$. The points Q and Q' represent configurations at which both of V and Ω vanish.

the counter-clockwise direction; its centre oscillates with a small amplitude about the tube centreline, with its major axis swinging about $\theta = 0$.

The negative sign of V in the range of $0 < \theta < \theta^*$ at $Y = 0$ for oblate spheroids is in contrast to its positive sign for prolate spheroids in that range (see figures 6 and 9). As mentioned earlier, a finite lateral velocity of an ellipsoid in tube flow is undoubtedly due to wall effects. Based on the lubrication theory, the positive lateral velocity of prolate spheroids may be explained in terms of the distribution of pressure generated in the gap regions between the tube wall and the particle, i.e. the reduced pressure acting on the upper side of the particle and the enhanced pressure on the lower side (see figure 2*h* in Secomb & Hsu 1993). Although similar arguments seem to also apply for oblate spheroids, their lateral velocity is negative.

In order to explain this phenomenon, we plot the velocity vectors and pressure contours in the plane of symmetry and the pressure contours on the particle surface in figure 11, for the oblate spheroid with $a = c = 0.7, b = 0.175$ at $Y = 0$ and $\theta = \pi/24 (< \theta^*)$. A dominant feature is drastic variations in the pressure distribution on the particle surface near both ends of the principal axis c, close to the sidewall; as the lubrication theory predicts, pressure on the particle near the sidewall is positive at the downstream part, and negative at the upstream part (see figure 11*b*,*c*). Although this pressure distribution does not produce any net force on the particle in the case of $Y = \theta = 0$, an inclined particle as shown in figure 11 may experience a force in the x_2-direction: for the downstream part, the width of the gap between the particle and the wall is narrower at the upper than at the lower end, so that a net downward force acts on the particle, because the lubrication force is increased in a narrower gap. Similarly, a net downward force also acts on the particle on the upstream part near the sidewall. These forces may result in the downward lateral motion of the oblate

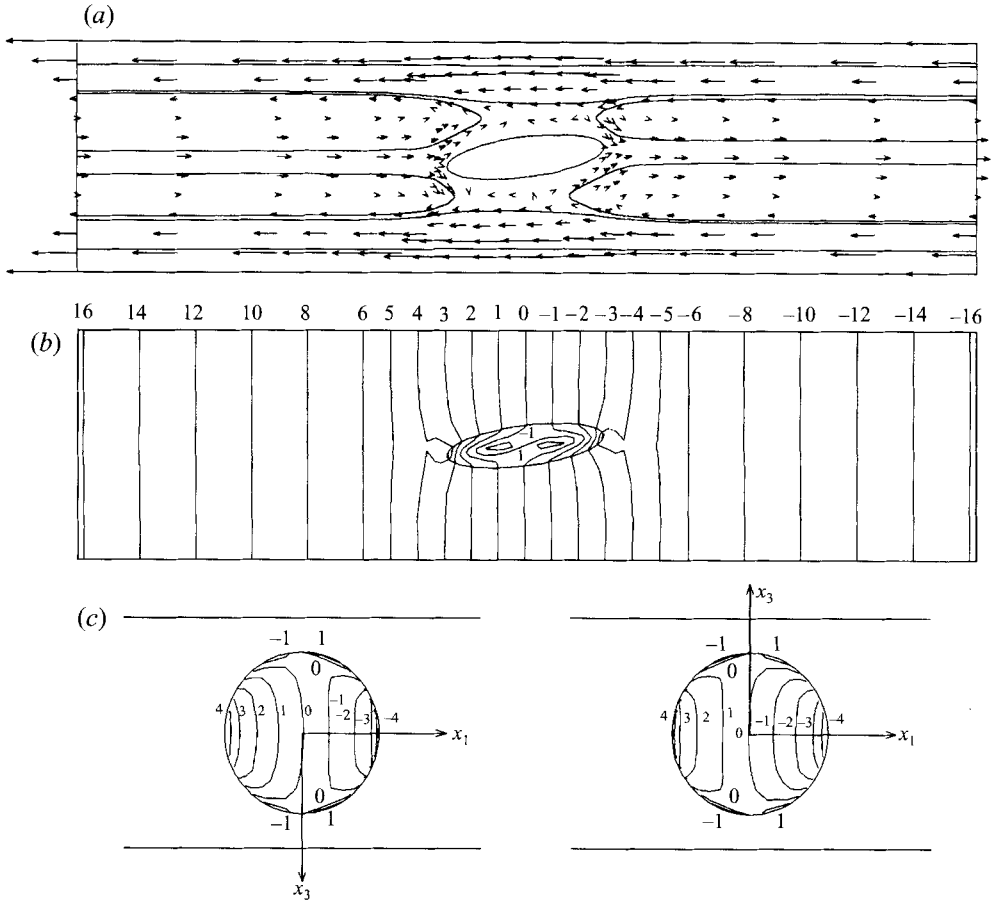

FIGURE 11. (*a*) Velocity vectors of the suspending fluid in the plane $x_3 = 0$ around an oblate spheroid with $a = c = 0.7$ and $b = 0.175$, located at the tube centreline with $\theta = \pi/24$. (*b*) Pressure contours in the plane $x_3 = 0$ and on the particle surface. (*c*) Pressure contours on the particle surface: left, top view; right, bottom view.

spheroid, for this configuration. For a more inclined spheroid, lubrication forces in the gap between the particle and the upper (lower) wall, not the sidewall, become larger, so that upward lateral motion may be induced, similarly to prolate spheroids.

It can be shown that, as in the case of prolate spheroids, the neutrally stable points P and P' exist in the regions of type (iii) motion (see figure 10), and these two points approach the origin with increasing particle size, until they coincide with the origin at $a = a^{\dagger}$ (see figure 8). Our computations show that the motion of an oblate spheroid with particle size above the critical value is significantly different from that of smaller spheroids.

As an example of the motion of oblate spheroids with $a > a^{\dagger}$, figure 12 shows velocity vectors and some representative trajectories of a spheroid with $a = c = 0.8$ and $b = 0.2$. Figure 12 suggests that a particle at any initial configurations except that in the region of type (ii) motion eventually approaches the points R_1, R_2, R_3 or R_4, depending on the initial configuration (type (v) motion). All these points represent a configuration at which the particle is slightly off the centreline with its principal axis a somewhat deflected from the undisturbed flow direction toward the tube

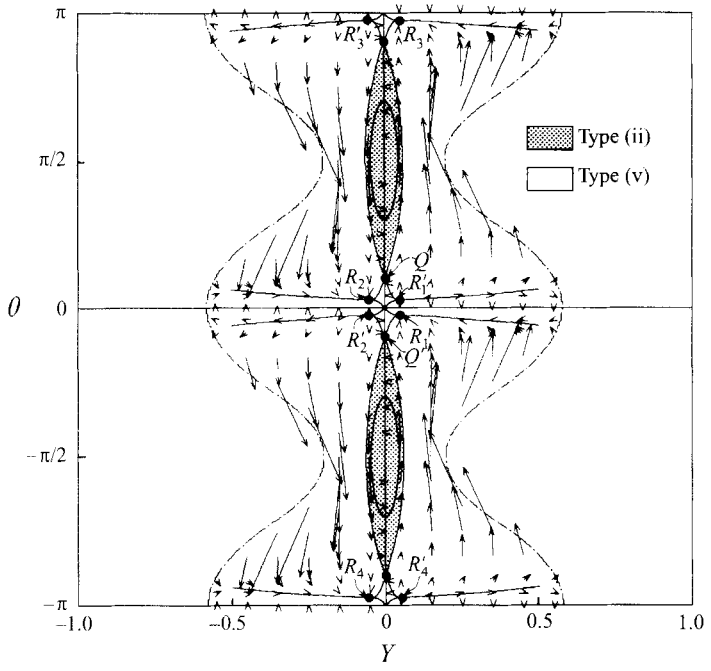

FIGURE 12. Vectors (V,Ω) for an oblate spheroid with $a = c = 0.8$ and $b = 0.2$. The points R_1, R_2, R_3 and R_4 represent stable equilibrium configurations while R_1', R_2', R_3' and R_4' are unstable.

centreline. Figure 13 shows the velocity vectors of the suspending fluid and pressure contours for an oblate spheroid with $a = c = 0.8$ and $b = 0.2$ near the configuration corresponding to the point R_1. It is interesting that for large oblate spheroids there is a stable configuration that is different from the equilibrium configuration expressed as $(Y,\theta) = (0,0)$. Note that the origin in figure 10 is neutrally stable, while the origin in figure 12 is unstable.

4.3. *General ellipsoids*

As may be expected from §4.1 and §4.2, it is found that the behaviour of an ellipsoid freely suspended in tube flow can be divided into four classes (a)–(d), depending on the presence or absence of points P and Q in plots of particle velocities (V,Ω) in the (Y,θ)-plane (table 1). The point P represents the configuration at which both of (V,Ω) vanish for an ellipsoid with its major axis aligned with the undisturbed flow direction. The point Q represents the configuration at which (V,Ω) vanish for an ellipsoid located at the tube centreline, the presence of which indicates the possibility of type (iv) and type (v) motions. In the case when point P is present and point Q is absent, type (i), type (ii) or type (iii) motion can occur depending on the initial configuration (class (a), see figures 6, 9*a*). When both points P and Q are absent, there are type (ii) and type (iii) motions (class (b), see figure 9*b*). When both points P and Q are present, type (iv) motion can occur in addition to type (i)–(iii) motions (class (c), see figure 10). When point P is absent and point Q is present, type (ii) motion and type (v) motion can occur (class (d), see figure 12).

In §4.1 and §4.2, we showed that small prolate spheroids are classified in class (a) and large prolate spheroids are in class (b), while small oblate spheroids are in class

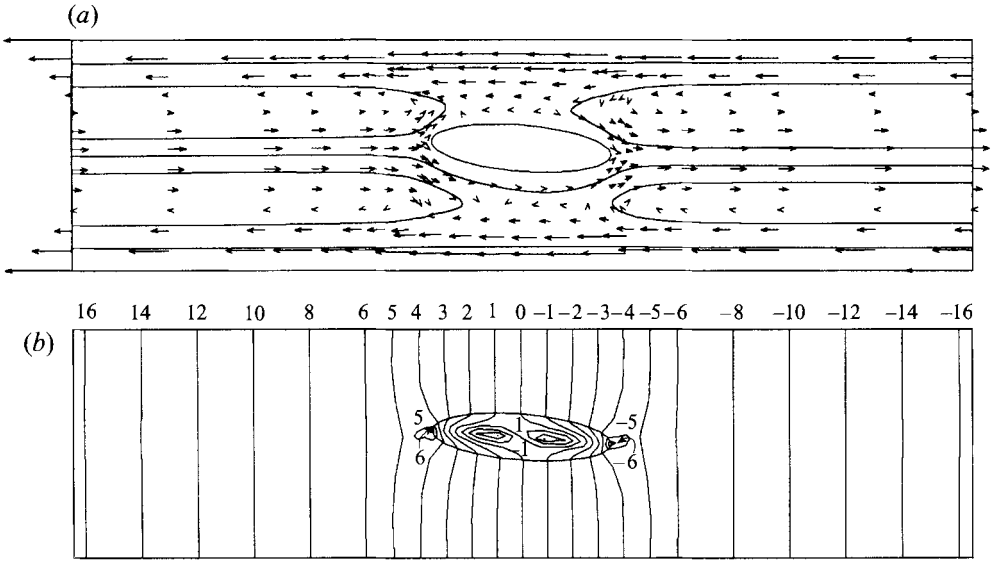

FIGURE 13. (*a*) Velocity vectors of the suspending fluid in the plane $x_3 = 0$ for an oblate spheroid with $a = c = 0.8$ and $b = 0.2$, at a stable equilibrium configuration corresponding to the point R_1 in figure 12. (*b*) Pressure contours in the plane $x_3 = 0$ and on the particle surface.

	Point Q: absent	Point Q: present
Point P: present	(a): type (i) motion type (ii) motion type (iii) motion	(c): type (i) motion type (ii) motion type (iii) motion type (iv) motion
Point P: absent	(b): type (ii) motion type (iii) motion	(d): type (ii) motion type (v) motion

TABLE 1. Classification of the behaviour of an ellipsoid in tube flow and possible types of particle motion.

(c) and large oblate spheroids are in class (d). In the present section, we consider the classification of the behaviour of non-axisymmetric ellipsoids.

As representative examples of non-axisymmetric ellipsoids, we consider those with $a = 0.8$, $b = 0.2$ and various values of c. Figures 6 and 12 suggest that the particle behaviour is in class (a) for small c, whereas it is in class (d) for larger c. This prediction is confirmed in figure 14(*a*), which shows a plot of the Y-coordinate of point P, Y^*, and the θ-coordinate of point Q, θ^*, as a function of c, for $a = 0.8$ and $b = 0.2$. Since positive values of Y^* or θ^* imply the presence of point P or Q, respectively, we see that point P is present for $c < c^\dagger$ while point Q is present for $c^\ddagger < c$. Thus, figure 14(*a*) indicates that the particle behaviour is in class (a) for $c < c^\dagger$, and in class (d) for $c > c^\ddagger$. Figure 14(*a*) also suggests the presence of class (b) behaviour in the range of $c^\dagger < c < c^\ddagger$, in which both P and Q are absent. The presence of class (b) behaviour is shown by a numerical computation for an ellipsoid with $a = 0.8, b = 0.2$ and $c = 0.7$, where $c^\dagger < 0.7 < c^\ddagger$ (a plot of the results is

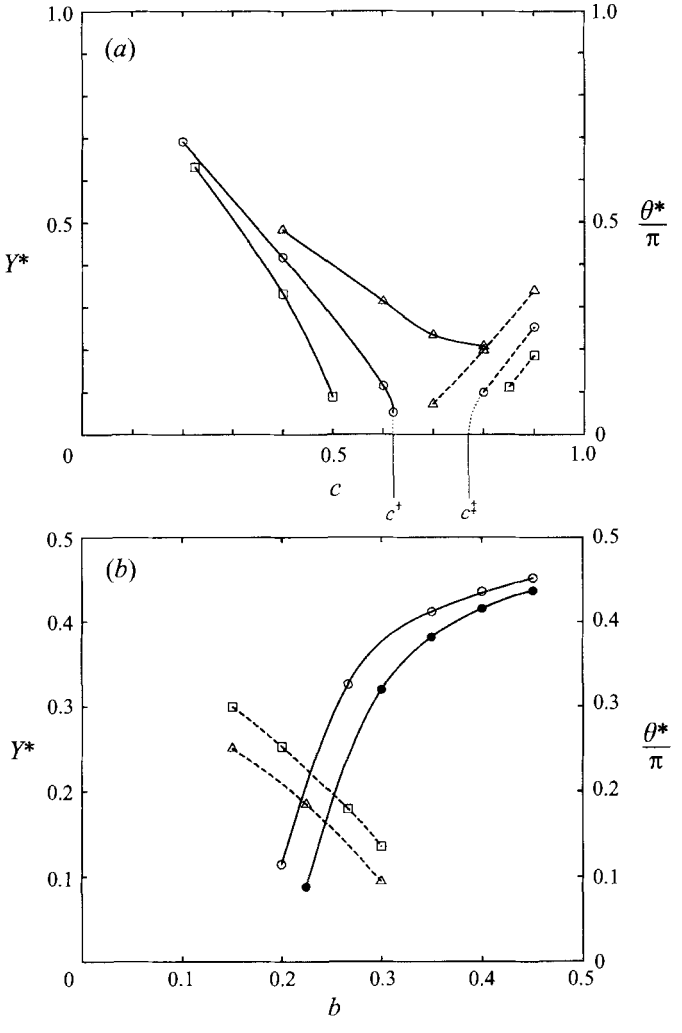

FIGURE 14. The Y-coordinate of point P, Y^* (——), and the θ coordinate of point Q, θ^* (- - - - -). (*a*) Ellipsoids with $a/b = 4$; ○, $a = 0.8$; □, $a = 0.9$; △, $a = 0.7$. $c^\dagger$ and $c^\ddagger$ represent the values of c at which Y^* and θ^* reach zero, respectively. (*b*) Various ellipsoids; ○, $a = 0.8$ and $c = 0.6$; •, $a = 0.9$ and $c = 0.5$; □, $a = 0.8$ and $c = 0.9$; △, $a = 0.9$ and $c = 0.9$.

not presented). Thus, the behaviour of ellipsoids with $a = 0.8$, $b = 0.2$ and various values of c is found to change from class (a) to class (b), followed by class (d) with increasing c.

In figure 14(*a*), the values of Y^* and θ^* for ellipsoids with $a = 0.7, b = 0.175$ and $a = 0.9, b = 0.225$ are also shown for comparison. It is suggested that $c^\dagger$ decreases and $c^\ddagger$ increases with increasing a for fixed values of a/b. Consequently, $c^\dagger$ and $c^\ddagger$ are further apart for ellipsoids with $a = 0.9, b = 0.225$ compared to the case of $a = 0.8, b = 0.2$, so that the behaviour of class (b) occurs in a wider range of c for $a = 0.9$, and $b = 0.225$. On the other hand, $c^\dagger$ seems to be larger than $c^\ddagger$ for $a = 0.7$ and $b = 0.175$, which results in the simultaneous presence of points P and Q in the range of $c^\ddagger < c < c^\dagger$ for ellipsoids with $a = 0.7$ and $b = 0.175$ (class (c)). Thus, in the case of $a = 0.7$,

$b = 0.175$ and various values of c, there is a class (c) behaviour for $c^{\ddagger} < c$, although it is not apparent whether a further increase of c monotonically decreases Y^* to zero.

In order to examine the effect of b on the particle behaviour, we plot Y^* and θ^* as a function of b, for several values of a and c (see figure 14*b*). It is seen that, in general, Y^* increases and θ^* decreases with increasing b, which is opposite to the tendency obtained for c (see figure 14*a*). Thus it is suggested that an increase (or a decrease) in b has a similar effect on the particle behaviour to a decrease (or an increase) in c. Since type (iii) motion is more likely to occur for smaller Y^*, figures 8 and 14 suggest that such an oscillatory motion is favoured for ellipsoids with large a, small b and large c. On the other hand, type (iv) motion is more likely to occur for larger θ^*, suggesting that this type of motion is favoured in cases of small b and large c.

More systematic analyses are required to classify the particle behaviour in more detail, and to explore the dependence of the stable configuration points $R_1 - R_4$ on various parameters. More complicated motions of an ellipsoid in the cases when the configuration is not necessarily symmetric with respect to the (x_1, x_2)-plane are left for further studies.

5. Concluding remarks

It is well known that the bulk properties of a suspension of rigid non-spherical particles depend strongly on the orientation of the particles. As mentioned in the Introduction, any axisymmetric particle will remain indefinitely in any given closed orbit, and thus the distribution of particle orbits is completely determined by the initial distribution of orientations in the suspension (Jeffery 1922; Bretherton 1962), unless effects of fluid and particle inertia, Brownian motion, inter-particle interactions, non-Newtonian properties of the suspending fluid, etc. are taken into account. Among these effects, Leal & Hinch (1971) and Hinch & Leal (1972) examined the effect of Brownian motion, and Brady and coworkers considered inter-particle interactions in studying suspension rheology of prolate spheroids (Claeys & Brady 1993*a–c*). Pozrikidis and coworkers have extensively studied the motion of ordered suspensions of liquid drops and their rheological properties, with and without the presence of boundary walls, and pointed out the significance of the boundaries on the structure and effective rheological properties of an emulsion (Zhou & Pozrikidis 1993*a,b*; Li, Zhou & Pozrikidis 1995).

For tube flow, the present study suggests several possible types of motion of single ellipsoids, and shows that an ellipsoid in tube flow will mostly exhibit periodic motions whose orbits are determined by the initial condition. Exceptions are type (i′), (ii′) and (v) motions where particles will eventually attain particular geometrical configurations. In all cases, the additional pressure drop due to the presence of an ellipsoid was found to depend strongly on the lateral position and orientation of the particle, as well as on the axis ratios and the particle size (see for example figures 4 and 7). In order to relate these results to the bulk properties of suspensions, it is necessary to elucidate the stability of the particle motion and the distribution of the orientation and position of the particles.

This research was supported in part by a Grant-in-Aid for Scientific Research from the Ministry of Education, Science and Culture of Japan. The numerical computations were performed at the Data Processing Centre, Kyoto University, and the Computation Centre, Osaka University, Japan.

REFERENCES

BRETHERTON, F. P. 1962 The motion of rigid particles in a shear flow at low Reynolds number. *J. Fluid Mech.* **14**, 284–303.

BUNGAY, P. M. & BRENNER, H. 1973 The motion of a closely fitting sphere in a fluid filled tube. *Intl J. Multiphase Flow* **1**, 25–56.

CHEN, T. C. & SKALAK, R. 1970 Spheroidal particle flow in a cylindrical tube. *Appl. Sci. Res.* **22**, 403–441.

CHWANG, A. L. 1975 Hydromechanics of low-Reynolds-number flow. Part 3. Motion of a spheroidal particle in quadratic flows. *J. Fluid Mech.* **72**, 17–34.

CLAEYS, I. L. & BRADY, J. F. 1993*a* Suspensions of prolate spheroids in Stokes flow. Part 1. Dynamics of a finite number of particles in an unbounded fluid. *J. Fluid Mech.* **251**, 411–442.

CLAEYS, I. L. & BRADY, J. F. 1993*b* Suspensions of prolate spheroids in Stokes flow. Part 2. Statistically homogeneous dispersions. *J. Fluid Mech.* **251**, 443–477.

CLAEYS, I. L. & BRADY, J. F. 1993*c* Suspensions of prolate spheroids in Stokes flow. Part 3. Hydrodynamic transport properties of crystalline dispersions. *J. Fluid Mech.* **251**, 479–500.

CLIFT, R., GRACE, J. R. & WEBER, M. E. 1978 *Bubbles, Drops, and Particles.* Academic.

GOLDSMITH, H. L. & MASON, S. G. 1967 *Rheology, Theory and Applications*, vol. IV (ed. F.R. Eirich) pp. 85–250. Academic.

HAPPEL, J. & BRENNER, H. 1983 *Low Reynolds Number Hydrodynamics.* Martinus Nijhoff.

HINCH, E. J. & LEAL, L. G. 1972 The effect of Brownian motion on the rheological properties of a suspension of non-spherical particles. *J. Fluid Mech.* **52**, 683–712.

HINCH, E. J. & LEAL, L. G. 1979 Rotation of small non-axisymmetric particles in a simple shear flow. *J. Fluid Mech.* **92**, 591–608.

HSU, R. & GANATOS, P. 1994 Gravitational and zero-drag motion of a spheroid adjacent to an inclined plane at low Reynolds number. *J. Fluid Mech.* **268**, 267–292.

HSU, R. & SECOMB, T. W. 1989 Motion of nonaxisymmetric red blood cells in cylindrical capillaries. *J. Biomech. Engng* **111**, 147–151.

JEFFERY, G. B. 1922 The motion of ellipsoidal particles immersed in a viscous fluid. *Proc. R Soc. Lond.* A **102**, 161–179.

KIM, S. & KARRILA, S. J. 1991 *Microhydrodynamics: Principles and Selected Applications.* Butterworth-Heinemann.

LEAL, L. G. & HINCH, E. J. 1971 The effect of weak Brownian rotations on particles in shear flow. *J. Fluid Mech.* **46**, 685–703.

LEICHTBERG, S., PFEFFER, R. & WEINBAUM, S. 1976 Stokes flow past finite coaxial clusters of spheres in a circular cylinder. *Intl J. Multiphase Flow* **3**, 147–169.

LI, X., ZHOU, H. & POZRIKIDIS, C. 1995 A numerical study of the shearing motion of emulsions and foams. *J. Fluid Mech.* **286**, 379–404.

OBERBECK, A. 1876 Ueber stationäre Flüssigkeitsbewegungen mit Berücksichtigung der inneren Reibung. *J. Reine Angew. Math.* **81**, 62–80.

OLSON, M. D. & TUANN, S. Y. 1978 *Finite Elements in Fluids*, vol. 3, pp. 73–87. Wiley.

POZRIKIDIS, C. 1992 *Boundary Integral and Singularity Methods for Linearized Viscous Flow.* Cambridge University Press.

POZRIKIDIS, C. 1994 The motion of particles in the Hele-Shaw cell. *J. Fluid Mech.* **261**, 199–222.

SECOMB, T. W. & HSU, R. 1993 Non-axisymmetric motion of rigid closely fitting particles in fluid-filled tubes. *J. Fluid Mech.* **257**, 403–420.

SECOMB, T. W., SKALAK, R., ÖZKAYA, N. & GROSS, J. F. 1986 Flow of axisymmetric red blood cells in narrow capillaries. *J. Fluid Mech.* **163**, 405–423.

STOVER, C. A. & COHEN, C. 1990 The motion of rodlike particles in the pressure driven flow between two flat plates. *Rheol. Acta* **29**, 192–203.

SUGIHARA-SEKI, M. 1993 The motion of an elliptical cylinder in channel flow at low Reynolds numbers. *J. Fluid Mech.* **257**, 575–596.

SUGIHARA-SEKI, M. 1995 Effect of irregularities of vessel cross-section on vascular resistance. *Fluid Dyn. Res.* **17**, 1–11.

TÖZEREN, H. 1982 Torque on eccentric spheres flowing in tubes. *Trans ASME* E: *J. Appl. Mech.* **49**, 279–283.

TÖZEREN, H. & SKALAK, R. 1978 The steady flow of closely fitting incompressible elastic spheres in a tube. *J. Fluid Mech.* **87**, 1–16.

WAKIYA, S. 1957 Viscous flows past a spheroid. *J. Phys. Soc. Japan* **12**, 1130–1141.

WANG, H. & SKALAK, R. 1969 Viscous flow in a cylindrical tube containing a line of spherical particles. *J. Fluid Mech.* **38**, 75–96.

WEINBAUM, S., GANATOS, P. & YAN Z.-Y. 1990 Numerical multipole and boundary integral equation techniques in Stokes flow. *Ann. Rev. Fluid Mech.* **22**, 275–316.

ZHOU, H. & POZRIKIDIS, C. 1993*a* The flow of suspensions in channels: Single files of drops. *Phys. Fluids* A **5**, 311–324.

ZHOU, H. & POZRIKIDIS, C. 1993*b* The flow of ordered and random suspensions of two-dimensional drops in a channel. *J. Fluid Mech.* **255**, 103–127.

ZHOU, H. & POZRIKIDIS, C. 1995 Adaptive singularity method for Stokes flow past particles. *J. Comput. Phys.* **117**, 79–89.